A Preliminary Investigation into the Hydroelastic Behaviour of a Non-Rigidly Mounted Hydrofoil

D. Clarke[1], B.Anderson[1], P. Brandner[2], B. Kidd[3], S. Kanev[3]

[1] Defence Science & Technology Organisation,
506 Lorimer St. Fishermans Bend, Victoria Australia 3027
[2] Australian Maritime College,
P.O. Box 986, Launceston, Tasmania Australia 7250
[3] ASC, Mersey Rd. Outer Harbour, South Australia 5018

Abstract

A preliminary investigation into the behaviour of a non-rigidly mounted hydrofoil is described. The foil was excited by boundary layer turbulence and trailing edge vortex shedding. The investigation involved the development and commissioning of specialised equipment to mount a hydrofoil in the Australian Maritime College Cavitation tunnel to enable parameters such as the stiffness and clearances about the 1st torsion mode of the mounting shaft to be varied. Tests were performed on a NACA 0015 foil with 200 mm chord, an 8 mm blunt trailing edge and a span of 274mm. The affect of changing the stiffness and clearance parameters on the dynamic response of the foil were measured via a three-axis accelerometer mounted inside the foil.

Introduction

Through the system of linkages and bearings that allow the incidence of a hydrofoil to be adjusted there is potential for the mounting arrangement to have undesirable flexibility or some degree of un-controlled movement (free-play). The interaction of the hydrofoil with the flow is of interest under these conditions. It is commonly known that “lock-in” can occur on a hydrofoil where the vortex shedding frequency is close to a resonant frequency of the structure. The subsequent noise amplification can be detrimental to the clandestine nature of defence vessels or result in vibration which causes premature fatigue. This phenomenon is well documented in the literature, even for low aspect ratio foils in high Reynolds number flows, particularly in the case where the foil is rigidly mounted.

In the case of a non-rigidly mounted hydrofoil, that is when the foil is not mounted rigidly to the root but by a supporting structure that has clearances and a degree of flexibility, it is unclear how these parameters affect the performance of a hydrofoil. In order to improve our understanding of dynamic hydroelastic instabilities of non-rigidly mounted hydrofoils, an experimental program was initiated.

Experimental Overview

The general arrangement for the set of experiments is shown in Figure 1. The test hydrofoil was mounted vertically in the Australian Maritime College (AMC) Cavitation Tunnel. The cavitation tunnel, located in Launceston, Tasmania has a test section with dimensions of 0.6m x 0.6m x 2.6m. The tunnel has a maximum flow speed of 12m/s and an adjustable pressure range from 0.04 to 4.0 atmospheres.

Figure 1 shows the hydrofoil model mounted to the Dynamic Foil Mount (DFM), which is located external to the test section. The span of the hydrofoil was chosen to be compatible with later testing which will involve the use of a divider in the tunnel test section to split the volume in two. With the divider in place, the foil will span from wall-to-wall, thus approximating two-dimensional flow across the foil. For this series of tests however, the test section divider was not available.

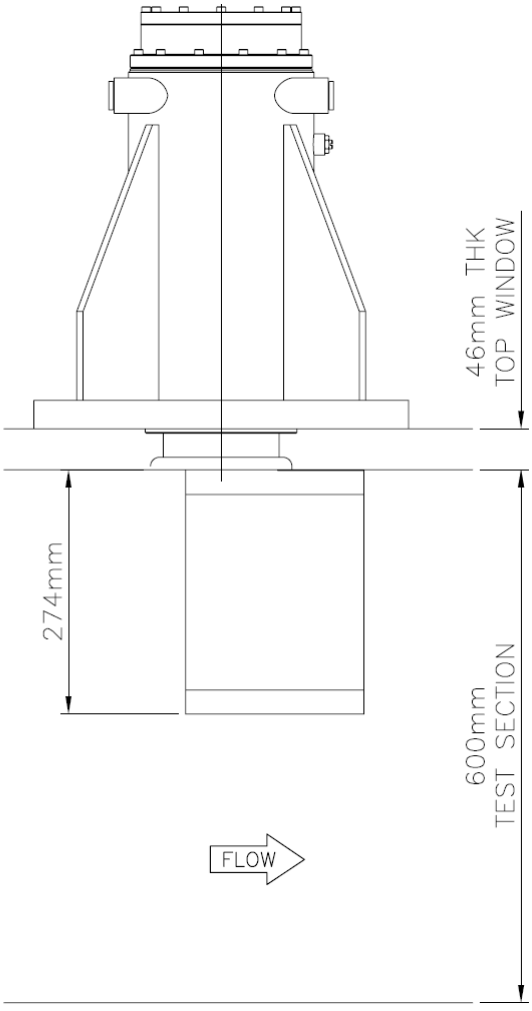

Figure 1. Experimental arrangement; NACA foil vertically mounted in the cavitation tunnel test section via the dynamic foil mount

Hydrofoil Description

The hydrofoil used in this study was a NACA 0015, with a truncated chord length of 200 mm, a blunt trailing edge thickness of 8 mm and a span of 274 mm. The trailing edge was designed for vortex shedding to occur and thus provide a suitable excitation source to commission the equipment. The axis of rotation of the foil, shown in Figure 2, was located at 20% of the chord. The foils were manufactured from aluminum with internal ribs to increase the stiffness. The voids of the foil were filled with foam to minimise the foil mass when submerged.

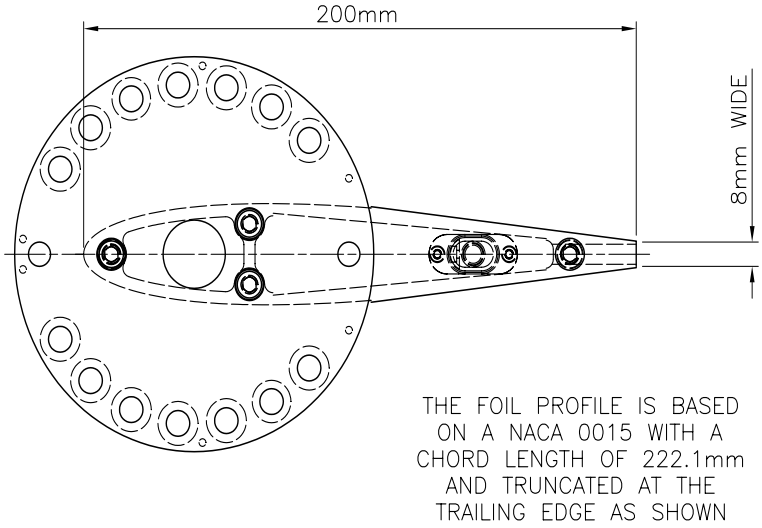

Figure 2. Top view of foil attached to mounting flange

Test Parameters

The parameters varied in the experiment included: the free-stream velocity, ranging from 1.8 m/s to 11.1 m/s (Reynolds numbers 0.4 - 2.2x10^6); clearances defined by the distance between the two stops on the dynamic foil mount, ranging from 0.02 mm to 1.03mm (equating to an angular range of 0.018 to 0.95 degrees); and the torsional stiffness of the rotational component of the DFM, which is defined by the thickness of the flexure neck shown in Figure 4. The characteristic dimension of the flexure neck ranged from 8mm to 16mm.

Turbulence Transition Strips

The hydrofoil was tested with and without trip strips to examine the influence of boundary layer condition on the interaction. The trip strips, designed to promote transition of the flow from laminar to turbulent, were adhesive studs applied to the model. The studs were cut from material manufactured by 3M, which allows them to be applied to the model in an efficient manner. Located 25 mm from the leading edge, the studs were circular in shape with dimensions of 1.25 mm diameter, 0.16mm in height and were spaced 4mm apart (centre to centre).

The trip strip used in these investigations was designed to transition the flow for velocities greater than 2.5 m/s. The technique described by Braslow and Knox (1958) was used to calculate the height of the stud at the specified chord-wise location. The results of by Von Doenhoff and Horton (1958) were used to determine a suitable value for the roughness Reynolds number, R_k, calculated to be 200. The resulting height for the roughness element was 0.16mm; this is approximately one and a half times the momentum thickness at the corresponding location and speed as calculated by the airfoil software XFOIL (Drela, 1989).

Accelerometer Description

In this series of tests the response of the hydrofoil was measured via an Endevco *65-100* triaxial accelerometer mounted internally to the hydrofoil model in a waterproof housing. The accelerometer was mounted close to the trailing edge with its y-axis oriented with the lateral motion of the foil. It was recognised that for future work at least two accelerometers would be necessary to assist in discerning the rotational mode from lateral modes.

Dynamic Foil Mount Description

In order to simplify the study of the influence of flexibility and clearances in the mounting system of a hydrofoil, a single degree of freedom, that being rotation, was selected. The aim was to isolate this degree of freedom so that its resonant frequency was not influenced by other resonant frequencies of the structure. Thus the key design requirement of the DFM was to maximise the stiffness of the rig with minimum mass of the rotating section. The DFM was designed to allow a hydrofoil to rotate about its span-wise axis.

The DFM consists of a rigid canister with a modular interior. The foil is mounted to a shaft; the shaft is held by two deep groove ball bearings 300mm apart, one of which acts as a thrust bearing. As can be seen in Figure 3 the bearing housings are held in the canister via a series of large diameter precision-machined tubes that are clamped in position when the lid of the canister is tightened. It was acknowledged at the outset that it is undesirable to have ball bearings in a system designed to study clearances, as they require clearances themselves. This limitation was accepted for the initial phase of testing in order that the rest of the rig could be tested and some preliminary results acquired. This will be the subject of future design improvements.

The rotational stiffness of the shaft is thus controlled by the flexure and the clearances by the stops, shown in Figure 4. The diameter of the shaft for the initial tests was limited by the size of the available stainless steel bearings; however the DFM canister was designed to accommodate possible bearing replacements. The shaft is connected to a T shaped bracket; the rotation of the T-bracket is controlled by either a flexure or a set of adjustable stops. The flexure or stops are fixed to the main canister via the upper bearing housing.

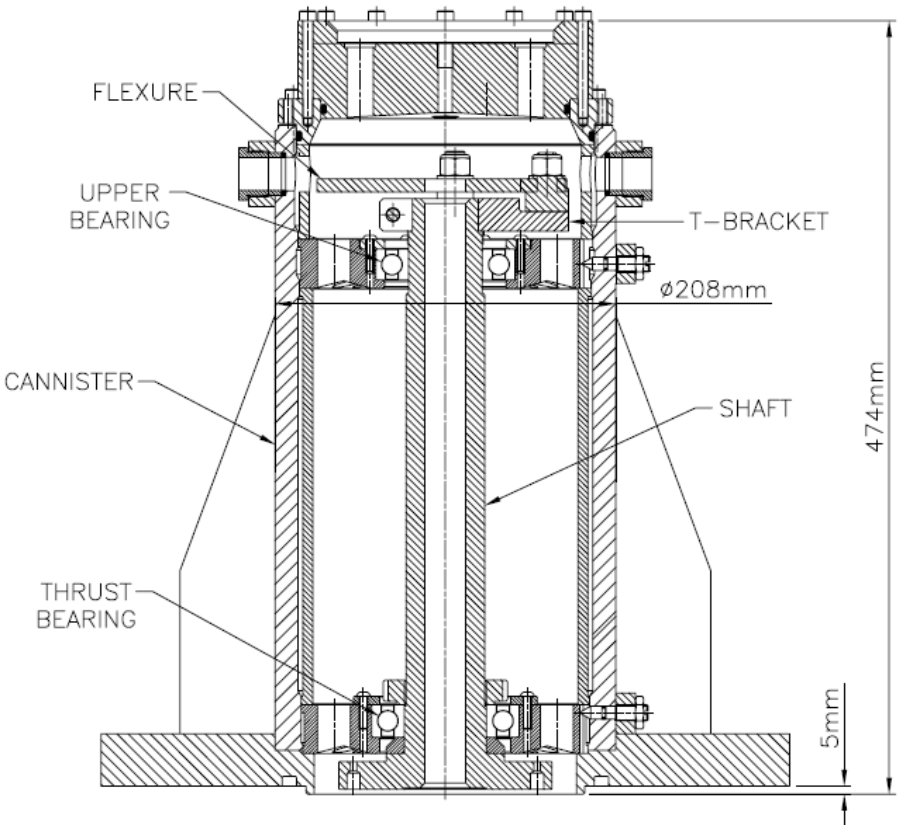

Figure 3. Side view of the dynamic foil mount

Operational Modal Analysis

A modal analysis of the DFM (Kanev, 2006) was conducted "in-air" to establish the resultant structural modes for the cases with the 8mm and 16mm flexures fitted and the case where "no flexure" was fitted. In the no flexure case, the flexure is replaced with a solid aluminium block to provide a rigid connection between the shaft and the canister. The general arrangement was the same as in Figure 1, except that the water was drained from the test section and a window removed to allow access to the model. The accelerometer mounted internal to the foil was used as a reference while another accelerometer of the same specification was used to perform roving measurements of the response from impact excitation on the experimental arrangement.

The fundamental rotational frequencies of the flexures were: 64 Hz for the 8mm flexure and 84 Hz for the 16mm flexure, both in air. The next nearest modes (in air) for the 8mm flexure and 16mm flexure were found to be 208 Hz and 211 Hz respectively and were attributed to lateral flapping and rocking of the hydrofoil about the dynamic foil mount bearings. In the case of the "no flexure" arrangement, the first mode corresponded to flapping motion about the lower thrust bearing; equivalent to the second mode in the 8mm and 16mm flexure cases. These measurements show that control of the rotational stiffness about the mounting shaft was achieved. The next nearest mode is attributed to flapping about the lower bearing, the frequency of which is some distance away from the rotational frequency in air.

Further tests with this arrangement are planned and will also include the use of a scanning laser vibrometer. This will enable the modes of the structure to be determined “in-water” with greater resolution than is easily performed with roving accelerometer measurements. Also, the effect due to added mass of the water will be incorporated into the modal analysis.

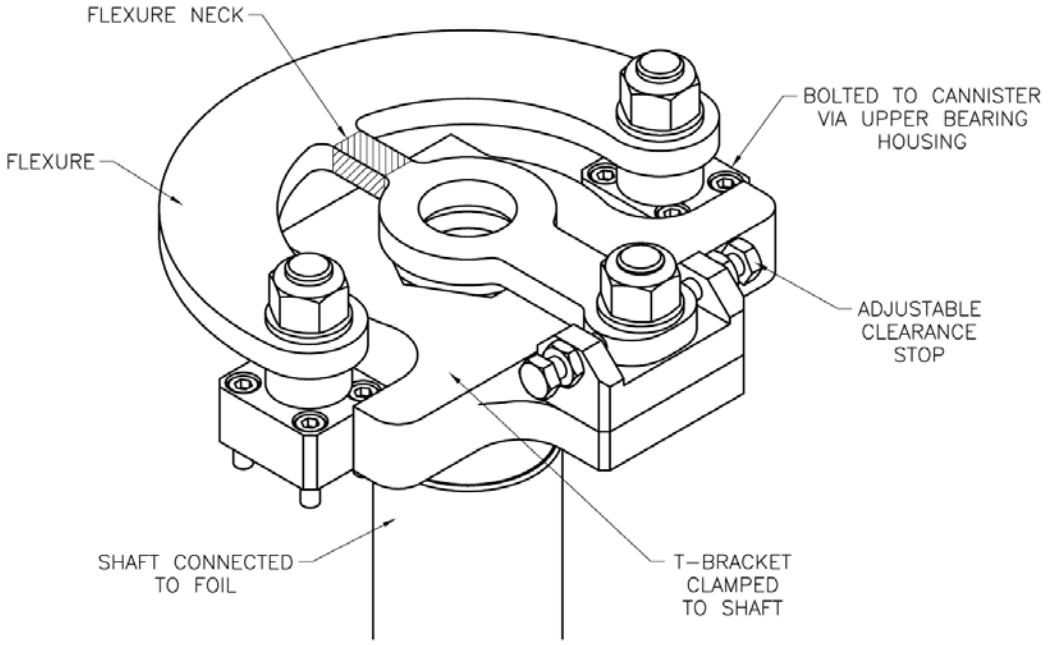

Figure 4. Schematic of the internal flexure design

Results and Discussion

The results from testing of the hydrofoil are contained in Figure 5 - 23 in the Appendix.

Figure 5 shows a comparison of the Strouhal number for hydrofoil tests with and without the turbulence transition trip strip and the clearances 0.00, 0.02 and 1.03mm. The Strouhal number was calculated by

$$S = \frac{fd}{U}$$

where f is the vortex shedding frequency identified from the accelerometer measurements, d is the trailing edge thickness (0.008m) and U the free-stream velocity. Blake (1986) incorporates the displacement thickness into the calculation of the Strouhal number for hydrofoils however this parameter was not measured in this set of tests. The figure clearly shows that tripping the hydrofoil results in a consistently lower Strouhal number than without the trip strips (assuming constant d). Based on the expression above, at U=4.1m/s, the Strouhal number for the tripped hydrofoil is approximately 0.175, which increases to 0.184 at U=8.5m/s, which then flattens out to 0.187 at U=12m/s. While the Strouhal numbers for the un-tripped foil, at the same free-stream velocities are 0.196, 0.203 and 0.205 respectively. The results for the tripped and non-tripped hydrofoil are distinct from each other however the difference would be reduced if a correction for displacement thickness was made. The

perturbations at approximately U=3, 6, and 8m/s are due to vortex shedding frequency passing through structural resonances.

Figures 6-13 show the dynamic response of the hydrofoil for free-stream velocities 2.5, 3.1, 4.1, 5.1, 6.1, 7.1, 8.1 and 11.1m/s and clearances 0.00, 0.02, 0.08, 0.20 and 1.03mm. No turbulence transition strips were used in these tests. The non-dimensional acceleration is given by

$$a' = \frac{a}{qAm}$$

where a is acceleration, $q = \frac{1}{2}\rho U^2$ is the dynamic pressure, A is the plan-form area and m is the foil mass (assumed unit mass). The figures show the $\log_{10}$ of the non-dimensionalised acceleration against frequency.

Figure 6 shows the hydrofoil response for the range of clearances given the free-stream velocity of 2.5m/s. This figure shows an overall increase in the background level for clearance 0.02mm. This is potentially due to the impacts creating broadband excitation.

Figure 7 shows the hydrofoil response at free-stream velocity 3.1m/s. Despite the difference in the vertical axis scale, it is clear that all clearances except the 0.00mm case had a similar level response. The increased response level of the 0.00mm clearance is due to the vortex shedding locking in to the first resonant mode.

Figure 8 shows the response level for clearance 0.08mm increasing towards that measured for clearance 0.02mm, which is distinctly separate from the two remaining clearances 0.20 and 1.03mm. The response level from clearance 0.00mm has decreased from that shown in Figure 7, which is attributed to the shedding frequency having passed through the structural mode. This does not return to its pre-resonance levels until approximately 5.0m/s as shown in Figure 14.

Figures 9 - 11 shows the amplitude of the frequency response for clearances 0.08, 0.20 and 1.03mm increasing with the velocity. At 11m/s Figure 13 shows almost identical frequency responses for all the measurements with a set clearance. Figure 12 shows the frequency response for the zero clearance case when the shedding frequency corresponds to the second structural resonance.

Figure 14 - 21 provide a different perspective on the data, much of it presented in the previous figures; they show two-dimensional contour plots of the $\log_{10}$ non-dimensional acceleration amplitude. These figures show the shedding frequency and its harmonics as a series of diagonal lines linearly proportional to velocity. The four vertical lines on the graphs show structural resonances similar to those identified in the “in air” operational modal analysis of the system. This is most clearly seen in Figures 20 and 21, which are the results for the 8 and 16mm flexure. The influence of the flexure on the frequency response is shown to only affect the first of these structural modes, which was one of the objectives of the DFM design.

In Figure 14, the non-tripped 0.00mm clearance case, resonances at 3 and 8m/s rapidly establish as the velocity increases. As the velocity continues to increase and the shedding frequency passes through the resonance, the response amplitude

gradually decreases. When the resonance is approached from the opposite direction, with decreasing velocity and thus decreasing shedding frequency, an almost identical plot is observed, hence the response shows no hysteresis.

Figure 15 shows a dramatic reduction in amplitude when the foil is tripped. The overall features are still present but the response when the shedding frequency coincides with the second structural resonance is barely visible.

Figures 16 - 19 show the results with clearances 0.02, 0.08, 0.20 and 1.03mm. The clearances have resulted in additional resonance modes that can also be seen in Figure 13. The amplitude of the frequency response above 750 Hz increases when sufficient energy is available from the flow to excite the hydrofoil. This suggests that the hydrofoil is highly damped.

Conclusions

This paper outlines the approach to an experimental program to investigate the dynamic hydroelastic instabilities of non-rigidly mounted hydrofoils. It reports on some preliminary results from the first series of tests. While some interesting observations have been made, further testing and analysis is required before conclusions can be drawn from this work. Several areas have been identified as next steps, these include:

- Implement the two-dimensional test arrangement i.e. manufacture and install the test section divider into the cavitation tunnel,
- In water modal analysis of the hydrofoil during testing is necessary to better characterise the response of the foil to fluid excitation,
- Investigate the DFM to determine any necessary design modifications to ensure the rotation single degree of freedom. Areas to be addressed include the bearing arrangements, and
- Perform a comparison between other trailing edge geometries, in particular a sharp ‘non-shedding’ trailing edge.

References

Braslow, A.L, Knox, E.C. *Simplified Method for Determination of Critical Height of Distributed Roughness Particles for Boundary-Layer Transition at Mach Numbers from 0 to 5*. NACA TN 4363, September 1958.

Blake, W.K., *Mechanics of Flow-Induced Sound and Vibration*, Academic Press Inc, New York, 1986.

Drela, M. *Xfoil: An Analysis and Design System for Low Reynolds Number Airfoils*. Proc. Low Reynolds Number Aerodynamics, June 1989, University of Notre Dame, USA, 1989.

Kanev, S., *Australian Maritime College Tom Fink Water Tunnel Hydrofoil Fixture Operational Modal Analysis March 2006*, ASC Engineering Report, April 2006.

Von Doenhoff, A.E., Horton, E.A. *A Low-Speed Experimental Investigation of the effect of a Sandpaper Type Roughness on Boundary-Layer Transition.* NACA Rep.1349, 1958.

Appendix

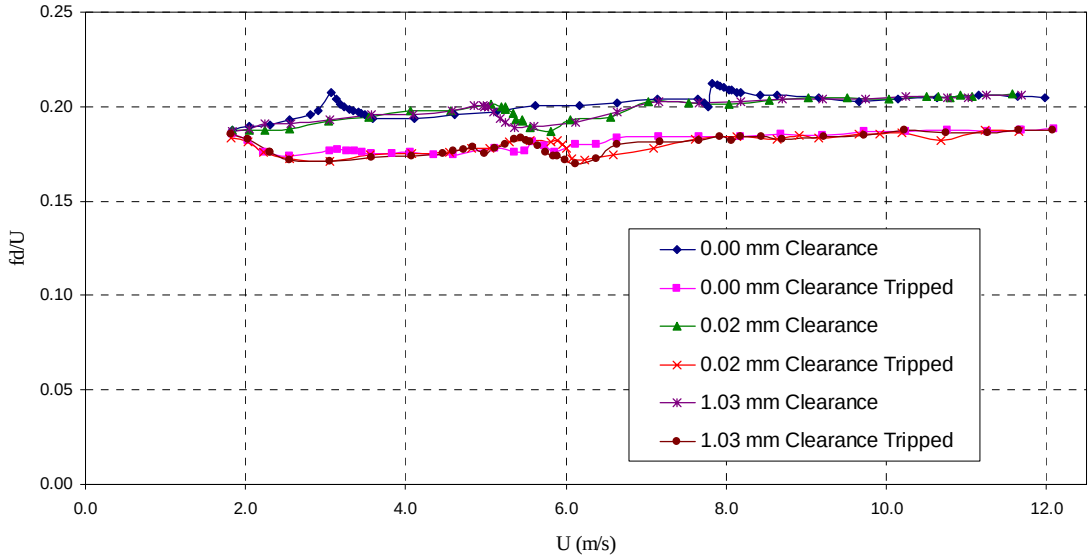

Figure 5. Comparison of Strouhal number for hydrofoil tests with and without turbulence trips for clearances 0.00, 0.02, and 1.03mm.

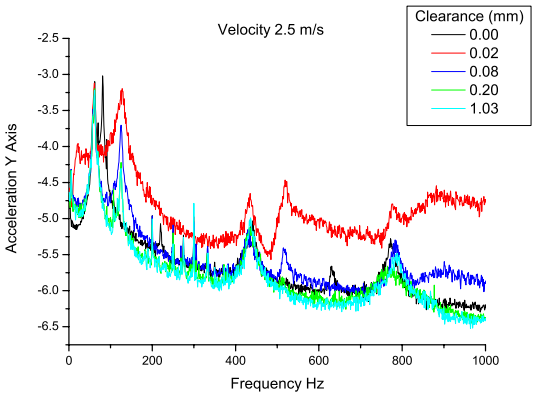

Figure 6. Non-dimensionalised y acceleration response at U=2.6m/s

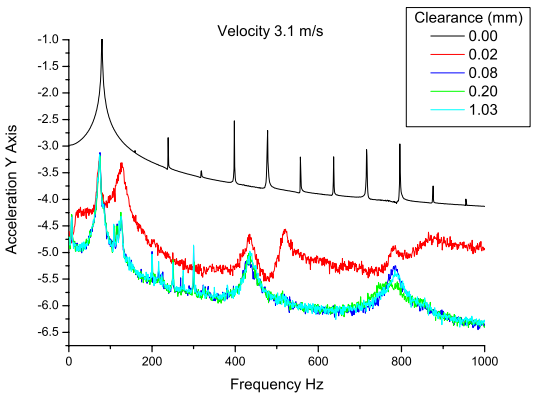

Figure 7. Non-dimensionalised y acceleration response at U=3.1m/s

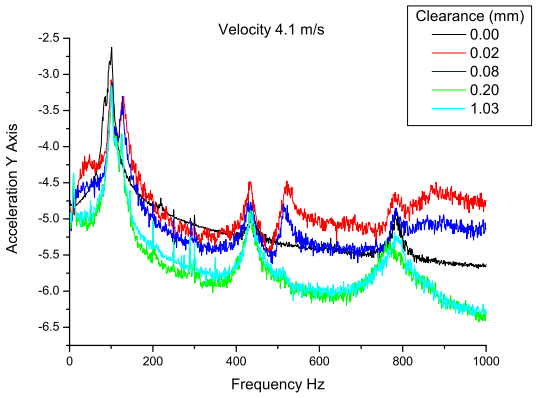

Figure 8. Non-dimensionalised y acceleration response at U=4.1m/s

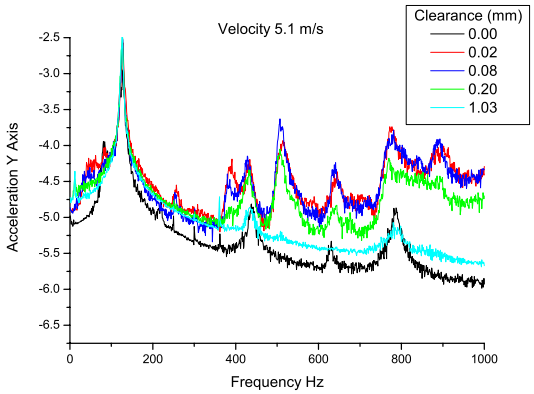

Figure 9. Non-dimensionalised y acceleration response at U=5.1m/s

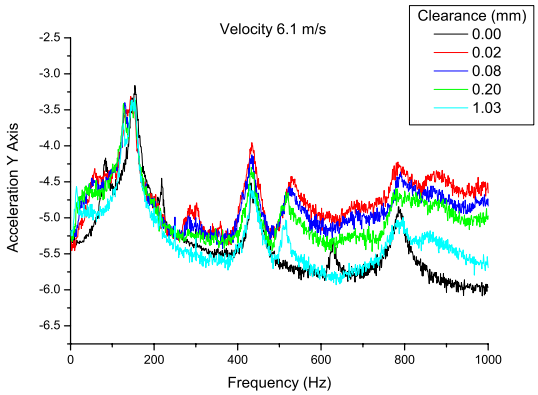

Figure 10. Non-dimensionalised y acceleration response at U=6.1m/s

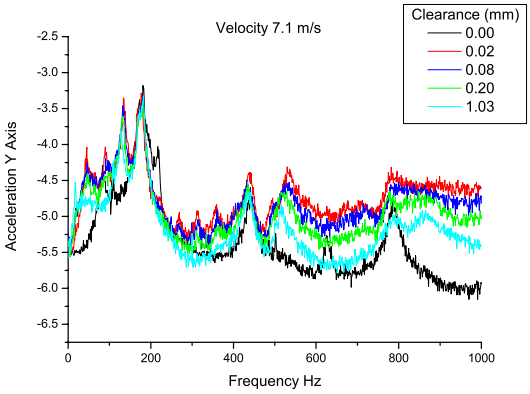

Figure 11. Non-dimensionalised y acceleration response at U=7.1m/s

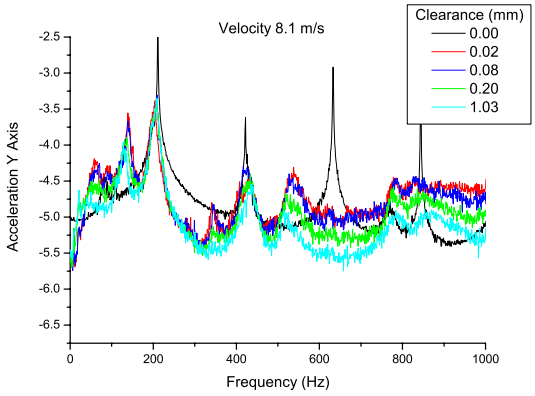

Figure 12. Non-dimensionalised y acceleration response at U=8.1m/s

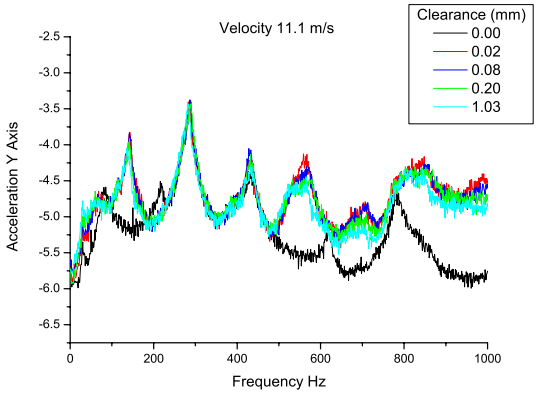

Figure 13. Non-dimensionalised y acceleration response at U=11.1m/s

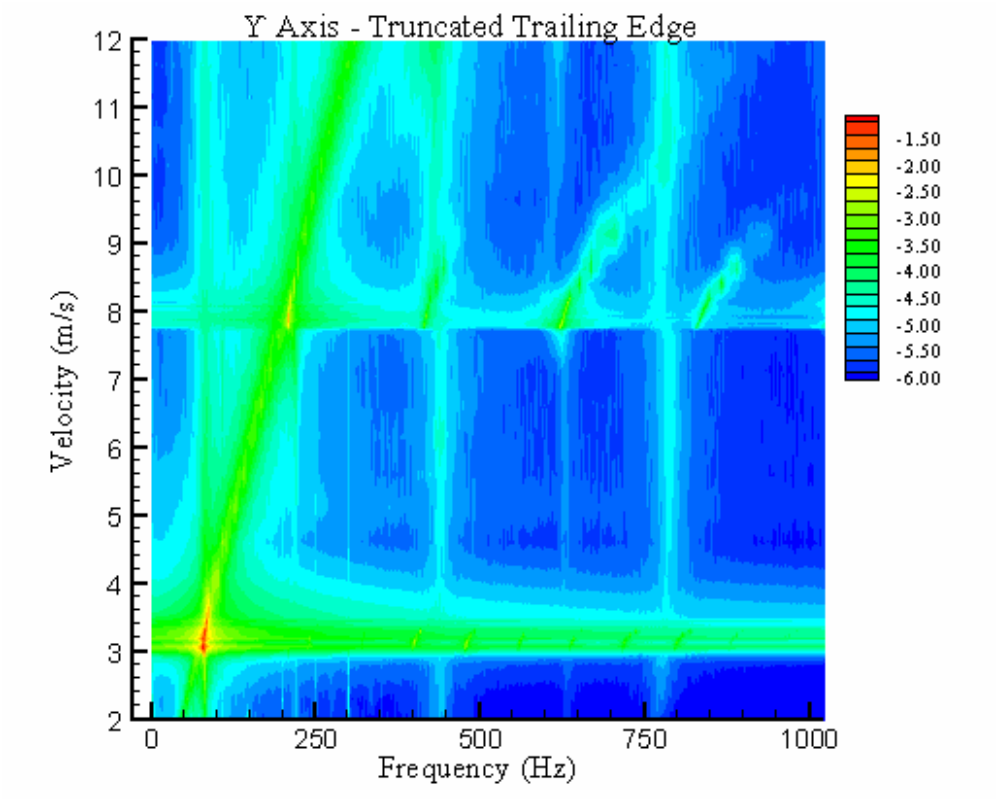

Figure 14. Acceleration amplitude, y-axis, clearance 0.00mm, untripped

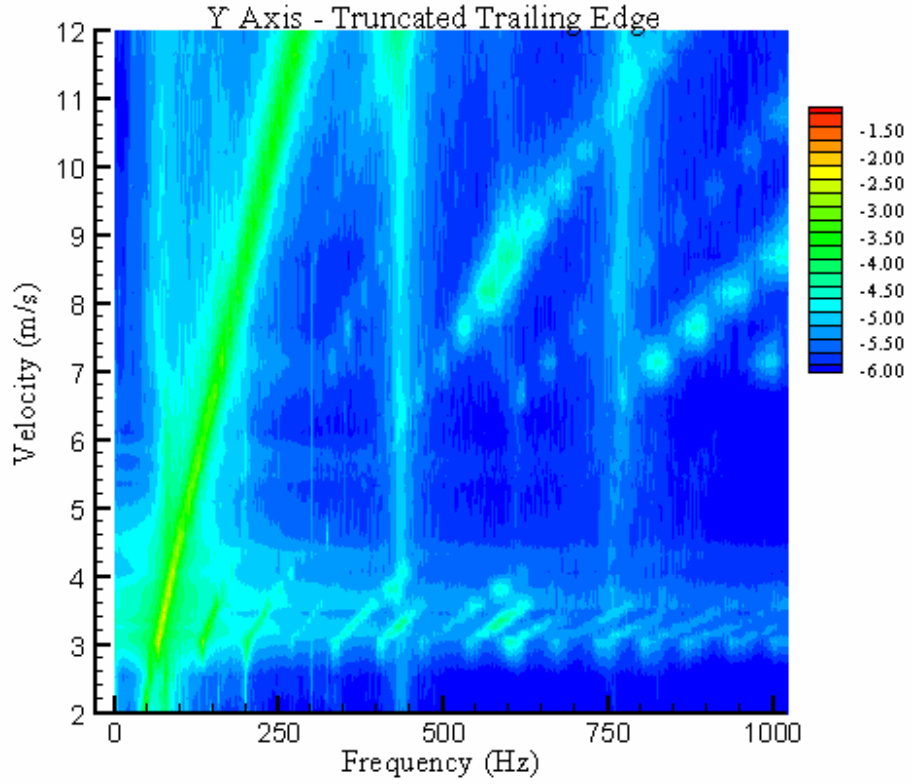

Figure 15. Acceleration amplitude, y-axis, clearance 0.00mm, tripped

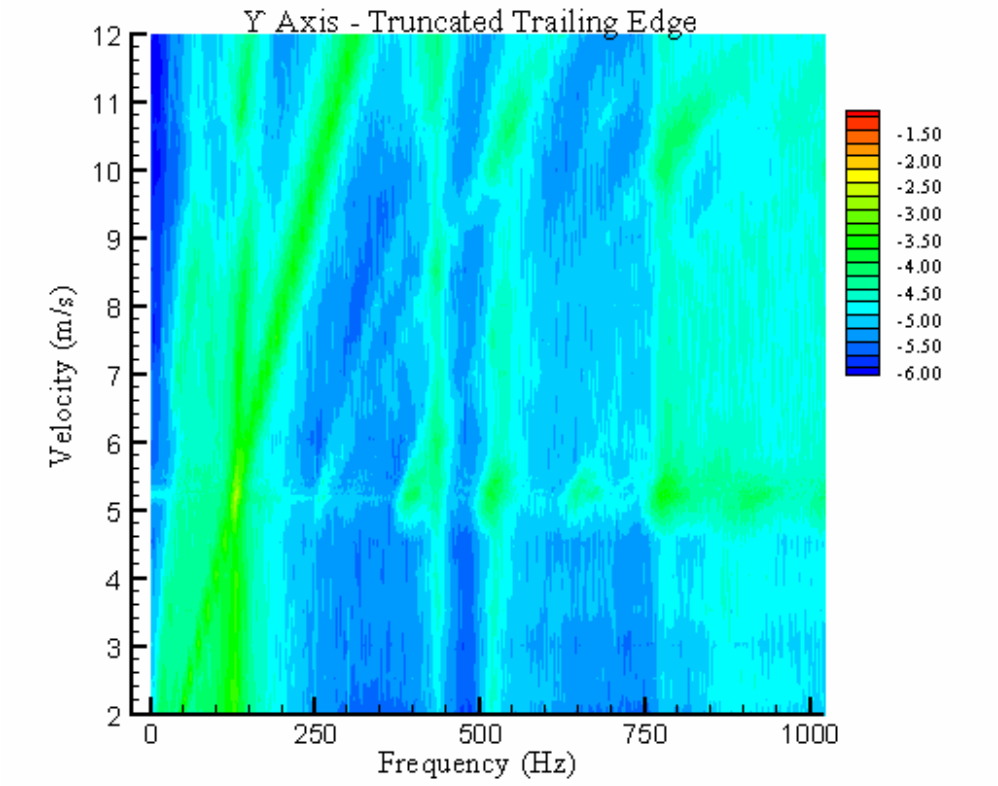

Figure 16. Acceleration amplitude, y-axis, clearance 0.02mm, untripped

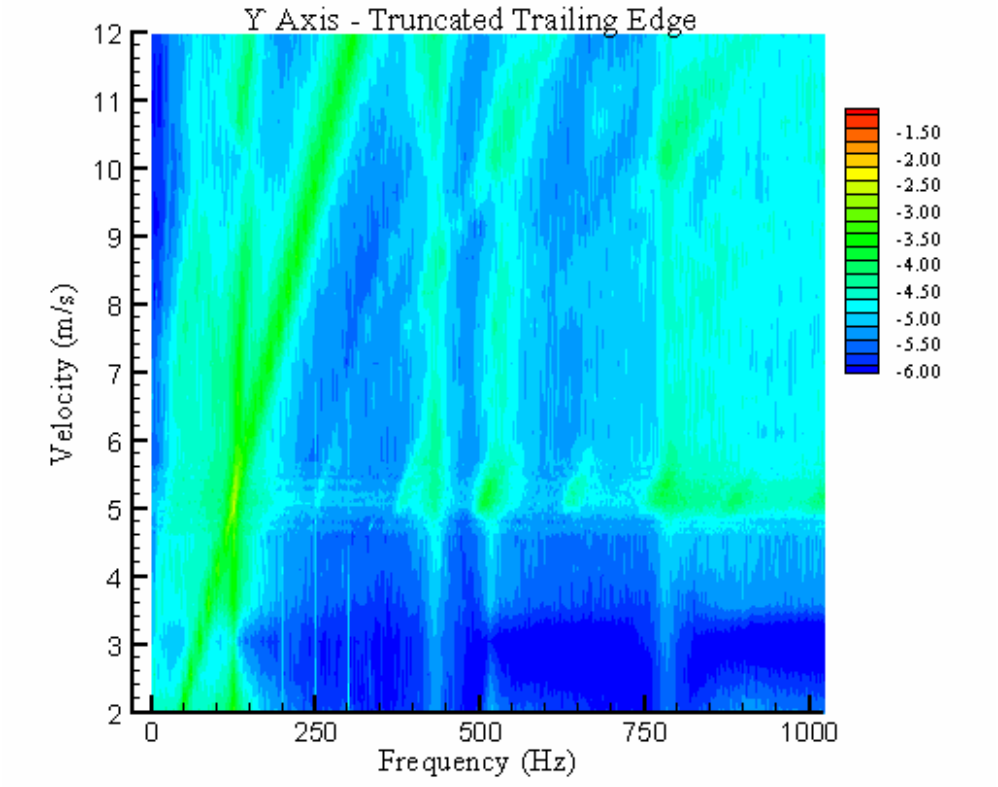

Figure 17. Acceleration amplitude, y-axis, clearance 0.08mm, untripped

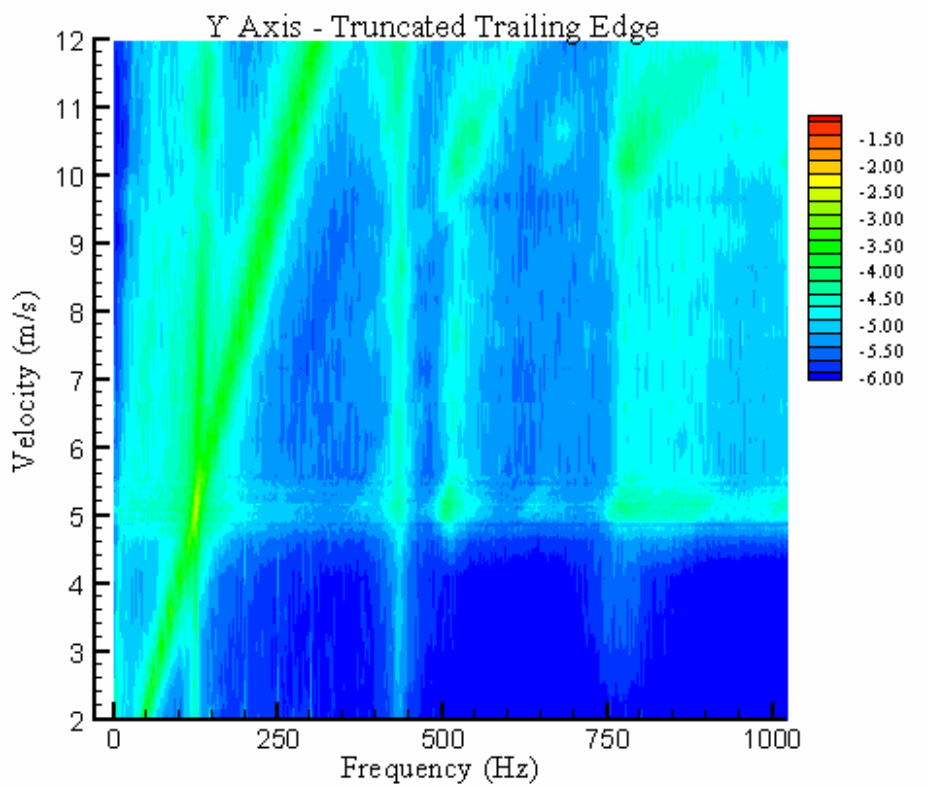

Figure 18. Acceleration amplitude, y-axis, clearance 0.20mm, untripped

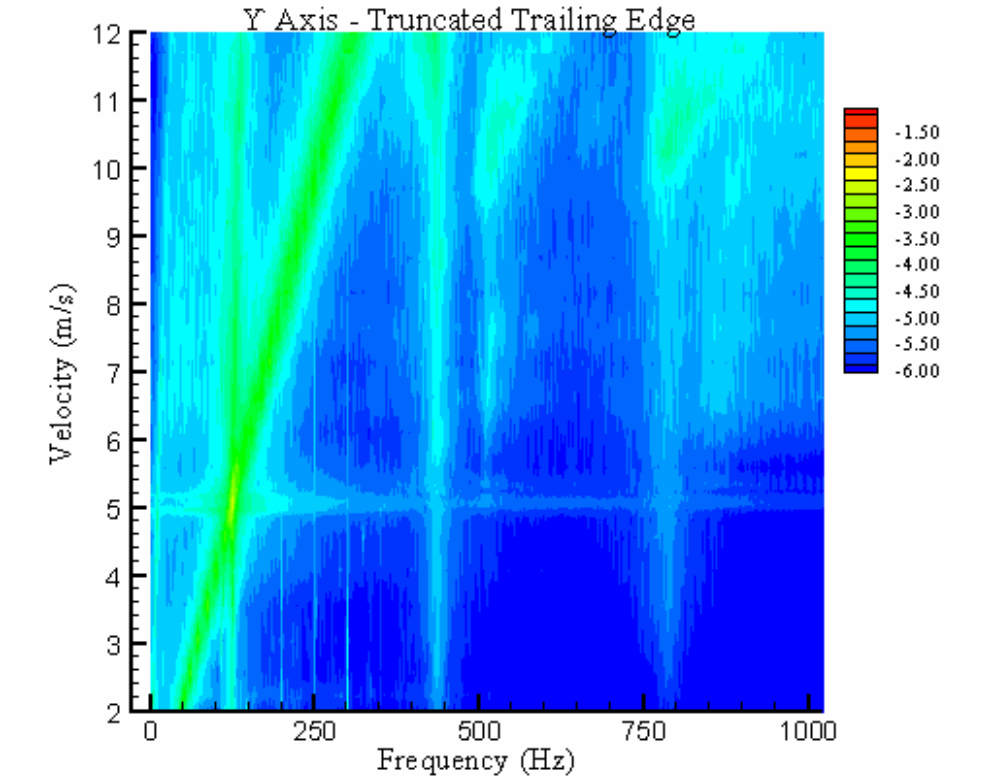

Figure 19. Acceleration amplitude, y-axis, clearance 1.03mm, untripped

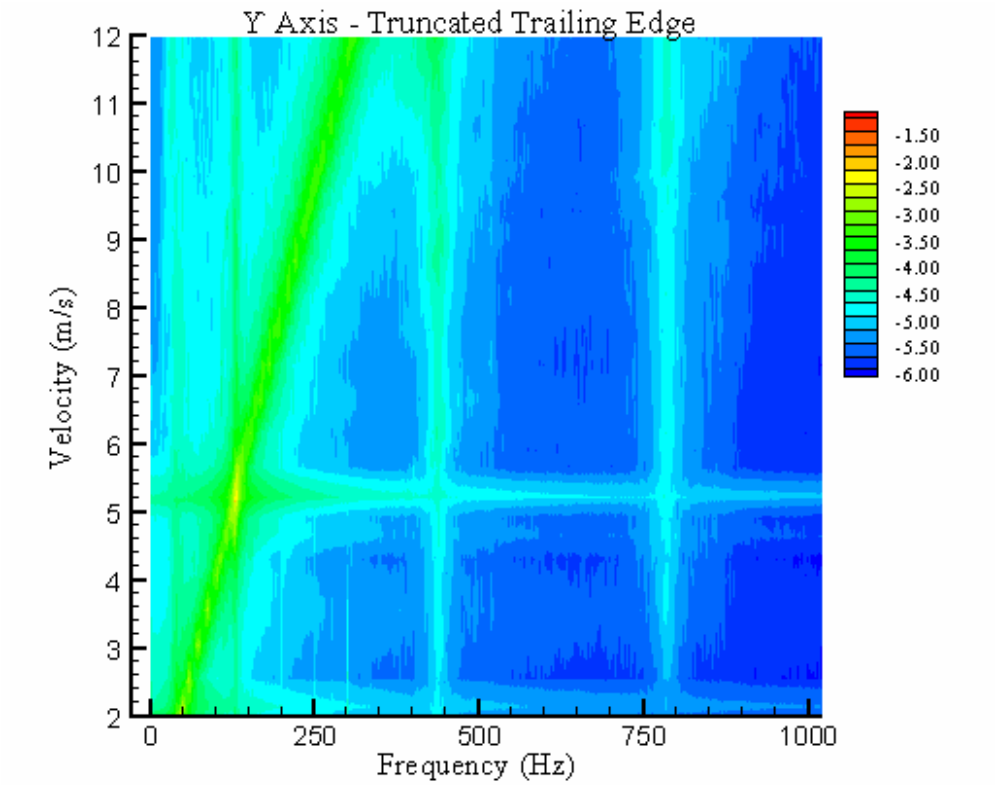

Figure 20. Acceleration amplitude, y-axis, clearance 0.00mm, untripped, 8mm flexure

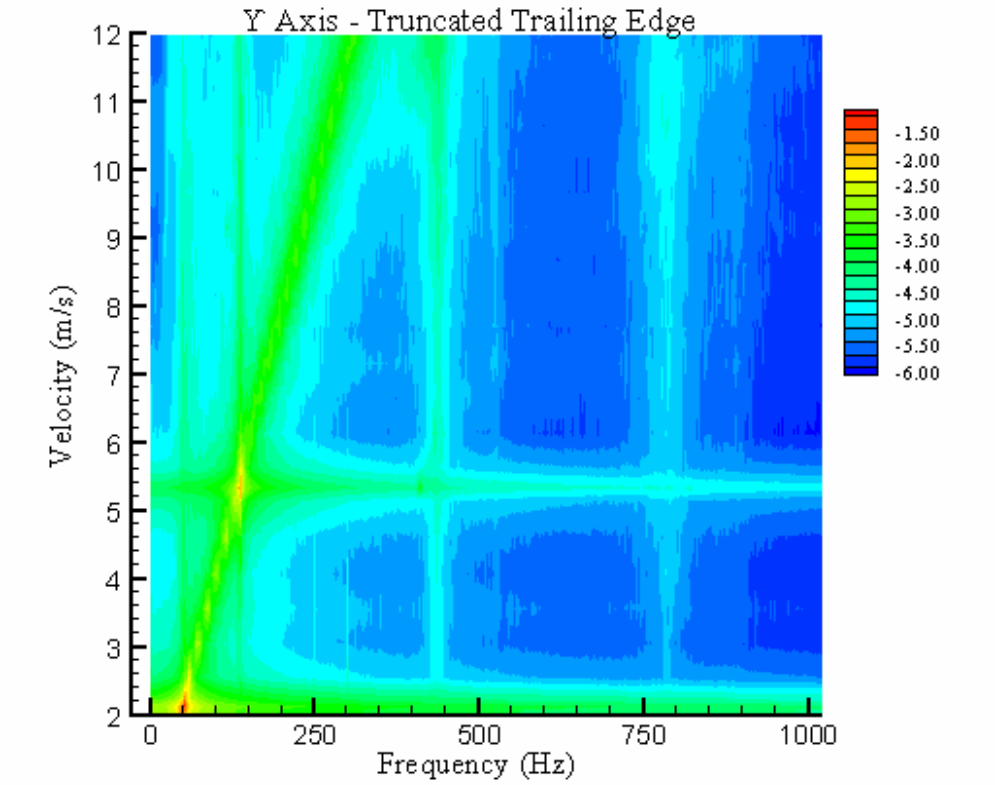

Figure 21. Acceleration amplitude, y-axis, clearance 0.00mm, untripped, 16mm flexure